

PAPER

Phase formation, magnetic and optical properties of epitaxially grown icosahedral Au@Ni nanoparticles with ultrathin shells

Cite this: *CrystEngComm*, 2013, 15, 2527

Lingfeng Huang,^a Aixian Shan,^{ab} Zhipeng Li,^c Chinpeng Chen^b and Rongming Wang^{*a}

The synergistic effect between the metallic elements in the core-shell nanostructures has attracted increasing interest. In the system of Au@Ni nanostructure, it is challenging to epitaxially grow Ni atoms on Au nanocrystals due to the large lattice mismatch. In this paper, Au@Ni core-shell nanostructures have been synthesized by a facile one-pot wet chemical method. The Ni shell is epitaxially grown on the (111) planes of the icosahedral Au cores. The diameter of the icosahedral Au core is about 10–20 nm and the thickness of the Ni shell is of only several nanometers, providing an ideal structure for the study of synergistic effect. The Curie temperature of the Ni shells is estimated to be lower than 400 K by the field-cooling/zero field-cooling $M(T)$ measurements. It is suppressed considerably from that of the bulk phase, mainly attributed to the finite size effect. The optical properties of the Au@Ni core-shell nanostructures are studied by absorption spectroscopy. The spectral blue-shift tendency is consistent with the results described by the plasmon hybridization theory.

Received 7th December 2012,
Accepted 18th January 2013

DOI: 10.1039/c3ce26980a

www.rsc.org/crystengcomm

Introduction

The synergistic effect of bimetallic nanomaterials with core-shell nanostructure has attracted great interest over the past few years.^{1,2} For a variety of reasons, the synthesis of magnetic noble bimetallic core-shell nanostructures with controllable sizes and uniform shell thickness remains a great challenge. In recent years, great efforts have been paid to synthesize various kinds of core-shell nanostructures with relatively controllable size, shape and composition.^{3,4} Among these structures, Au based core-shell nanostructures have aroused considerable interest for their optical,^{5,6} magnetic^{7,8} and catalytic⁹ applications. One of the hottest areas of research in Au based nanostructures is their special optical properties such as surface-enhanced Raman spectroscopy.¹⁰ Another important area of research in these nanostructures is their combination with magnetic elements.¹¹ The introduced magnetism and the modified magnetic properties of the shell make significant differences to the practical applications. For instance, the presence of magnetism favours the assembly of bimetallic nanoparticles (NPs).¹²

Methodologically, advances have been made in synthesizing core-shell nanostructures by wet chemical routes. For instance, the galvanic exchange method was created and applied in synthesizing several core-shell and alloyed nanostructures.^{13–16} Lately a new supramolecular route for the synthesis of core-shell nanostructures was reported, which made the synthesis of much smaller nanostructures feasible.¹⁷ Although the Au@Ni and Ni@Au nanostructures have great advantages and the synthetic methods of core-shell nanostructures have been developed for years, related reports are limited.

Recently, Ni@Au and Au@Ni nanostructures with an average size of tens of nanometers were successfully prepared in the oleylamine system.¹⁸ Also, the Ni@Au nanostructures were synthesized in reverse microemulsion, which was a galvanic exchange process between Ni and AuCl.^{4–19} Similarly, a one-pot wet chemical route had been reported for preparing Au@Co nanostructures *via* a noble-metal-induced reduction process using 4,4'-diaminodiphenyl ether (ODA) as both solvent and surfactant.²⁰ Though the Au based core-shell nanostructures have been synthesized, the large lattice mismatch still makes it a problem for the formation of the Ni shells epitaxially grown, in particular, over the Au surfaces. The synthesis of Au@Ni core-shell NPs with controllable size and uniform shape in a simple and clean system remains a challenge. In addition, a two-step reduction method has been reported for the synthesis of Au@Ni core-shell nanostructures.²¹ The size is over 100 nm and the shell thickness is

^aKey Laboratory of Micro-nano Measurement-Manipulation and Physics (Ministry of Education), Department of Physics, Beijing University of Aeronautics and Astronautics, Beijing 100191, P. R. China. E-mail: rmwang@buaa.edu.cn

^bDepartment of Physics, Peking University, Beijing 100871, P. R. China

^cBeijing Key Laboratory of Nano-Photonics and Nano-Structure (NPNS), Department of Physics, Capital Normal University, Beijing 100048, People's Republic of China

about tens of nanometres, too large to observe the synergistic effect in the system.

In this work, the Au@Ni core-shell nanostructures with uniform shape and thin epitaxial shell, 2–5 nm, were synthesized *via* a one-pot wet chemical process. The atomic structure and possible growth mechanism of the core-shell nanostructure have been investigated. Their magnetic and optical properties have also been investigated and discussed in terms of the synergistic effect.

Experimental

EG (ethylene glycol), PVP (poly-vinylpyrrolidone) (K-30), Ni(NO₃)₂·6H₂O (nickel nitrate), C₆H₅Na₃O₇·2H₂O (sodium citrate) and NaOH (sodium hydroxide) were purchased from Beijing chemical works. HAuCl₄·4H₂O (chloroauric acid) was purchased from Shenyang Jinke chemical reagent works. All reagents were analytical grade and used as received.

In a typical synthesis, 0.5 g PVP was dissolved in 15 ml EG, then a freshly prepared solution of C₆H₅Na₃O₇·2H₂O (5 mg in 1 ml of H₂O) was added into the EG solution, and then the mixed solution was sonicated for 15 min. After that, the mixed solution was heated to 185 °C under magnetic stirring and nitrogen bubbling in a flask. After 10 min, 5 ml HAuCl₄ (5 mg in 5 ml EG) was added with the speed of 300 ml h⁻¹. As the reaction proceeded, a homogeneous amaranthine solution was obtained. Then 5 ml Ni(OH)₂ (formed by 10.5 mg Ni(NO₃)₂·6H₂O and 5 mg NaOH dissolved in 5 ml EG) was added into the former solution at the speed of 100 ml h⁻¹ and kept at 185 °C for 1 h. The colour of the solution changed to black, indicating the formation of Ni shell. The product was collected by centrifugation and washed several times with ethanol.

The morphologies, structures and chemical compositions of the as-synthesized products were studied using X-ray diffraction (XRD, X'Pert Pro MPD system, Cu K α , λ = 0.154 nm), transmission electron microscopy (TEM, JEOL 2100F at 200 kV) equipped with an energy dispersive X-ray spectroscopy (EDS). TEM samples were dispersed on a Cu-grid coated with porous carbon films. Magnetic properties of the as-synthesized powder samples were measured with a SQUID magnetometer (Quantum Design). Optical properties of the products were studied using an ultraviolet and visible spectrophotometer (UV-3500, SHIMADZU Design).

Results and discussion

It is known that the epitaxial growth of Ni on the Au NPs is difficult for the large lattice mismatch between Au and Ni. Therefore, it is essential to characterize the microstructure of the Au@Ni NPs to make sure that the Ni shells are epitaxially grown. Meanwhile, the studies on the magnetic and optical properties are helpful to explore the synergistic effects between different elements in bimetallic NPs. In this work, the Au@Ni core-shell NPs are synthesized with the Au core of about 10 to

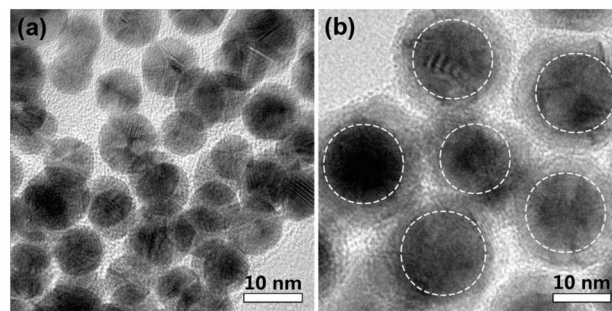


Fig. 1 TEM images of as prepared (a) Au cores; (b) Au@Ni nanostructures.

20 nm in diameter and the Ni shell of 2–5 nm in thickness. The Au cores are icosahedral with 20 (111) facets. The icosahedron morphology is a favourable structure for metallic/bimetallic NPs, which has been studied previously in FePt bimetallic nanostructures.^{22,23} Structurally, the icosahedron can be considered as a combination of 20 tetrahedrons. The Ni layers are formed by epitaxially growing along the [111] direction over the Au surfaces. Interestingly, the shape of icosahedron, remains even after the Ni shells are fully grown to cover the Au cores, favourably supporting the epitaxial growth instead of adsorption growth of Ni nanocrystallites. This point is confirmed by more evidence of morphology and structure from HRTEM characterizations.

Au@Ni core-shell nanostructures

The TEM image reveals the morphology of the Au core in Fig. 1a. The diameter of the Au NPs is about 10 nm in this image. The core@shell structure of the Au@Ni NPs with the central darker Au core and the lighter Ni shell is shown in Fig. 1b. The shell thickness of Ni is estimated at ~2 nm.

The XRD pattern for the Au@Ni NPs is shown in Fig. 2a. The diffraction peaks can be assigned to fcc-Ni and fcc-Au, in supportive of the presence of Ni and Au. The most intense diffraction peak for the Au is (111). This implies that [111] is the most preferential growth direction of the Au core as confirmed more directly by HRTEM later. The compositions are studied by EDS, shown in Fig. 2b, with the background signals of C and Cu originating from the supporting Cu-grid with a carbon film. The O signals may originate from the oxidation of Ni shells during the sample preparation. Atomic

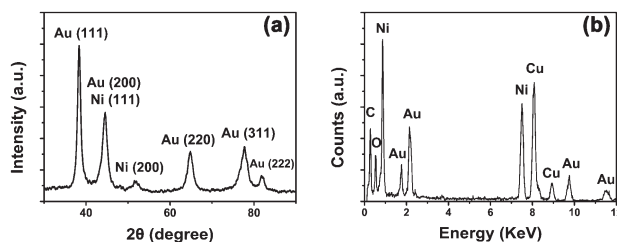


Fig. 2 (a) XRD pattern for the as-prepared Au@Ni NPs, indexed to Au (JCPDS no. 04-0784) and Ni (JCPDS no. 04-0850); (b) EDS analysis of the as-prepared Au@Ni NPs.

ratio of Au to Ni is about 25 : 75 in the EDS spectrum, which is in accordance with the ratio of the original reagents, indicating the effective reduction of Au and Ni precursors.

Structure of icosahedral Au NPs

To further clarify the icosahedral structure of the Au cores, HRTEM images taken at three different orientations are presented. Fig. 3a is a 2-fold symmetry projection viewed along the [100] axis. The corresponding (111) facets can be clearly seen as marked in the image. Fig. 3b is a 3-fold symmetry projection of another Au core, viewed along the [111] direction, and Fig. 3c is a 5-fold symmetry projection viewed along some direction, such as the [023]. By a tilted view angle away from the symmetric axis, the 5-fold symmetry projection appears to be slightly asymmetric. Fig. 3d–f are obtained by MacTamps atomic simulation using a model established by inputting the atomic coordinates and parameters with the Au icosahedrons of fcc structure. By changing the simulating direction of view in the computer, the symmetric patterns are completely regenerated corresponding to the HRTEM images shown in Fig. 3a–c, respectively. In other work, simulations have shown that icosahedron is one of the stable morphologies for small NPs of pure metals with an fcc lattice structure.^{24,25} There are quite a few examples, such as, Ag,²⁶ Pd²⁷ and Au²⁸ icosahedral NPs from less than 10 to about 200 nm, prepared by chemical methods.

Epitaxial growth of Ni shells

The HRTEM images indicate that the Au@Ni core-shell nanostructures are well-crystallized with the lattice fringes clearly visible, as shown in Fig. 4a and b. The shape of the Ni shell is remarkably consistent with the inner Au core. In Fig. 4a, the inter-planar spacing near the interfacial region is determined as 0.20 nm, corresponding to fcc-Ni (111) planes. The other one within the core region is about 0.24 nm in separation, corresponding to fcc-Au (111) planes. These two sets of fringes are in parallel. This is one of the evidences that the Ni shells are grown epitaxially over the Au surfaces. Moreover, Fig. 4b shows the Moiré Patterns in the region enclosed by the dash circle. The Moiré Pattern is even more

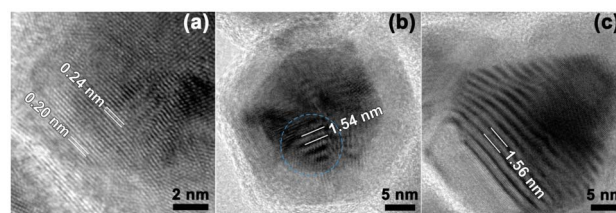


Fig. 4 (a) HRTEM image on one corner of an Au@Ni core-shell NP; (b) the Au@Ni icosahedral NP and (c) plate like NP with visible Moiré Patterns.

pronounced in Fig. 4c, a triangular Au@Ni nanoplate selected out from the icosahedral ones. The Moiré Pattern resulting from the lattice mismatch in the boundary at which Ni is epitaxially grown over the Au crystals. A more quantitative analysis shows indeed that these Moiré Patterns are attributed to periodical lattice matching at Ni–Au interfaces. According to the formula

$$D = \frac{d_1 d_2}{|d_1 - d_2|} \quad (1)$$

(1) the spacing of the Moiré Pattern (matching period) is calculated to be 1.49 nm by using the lattice constants of $d_1 = 0.2355$ nm for Au (111) and $d_2 = 0.2034$ nm for Ni (111). This matches the observed values of 1.54 nm in Fig. 4b, and 1.56 nm in Fig. 4c very well. It further demonstrates the epitaxial growth mechanism of Ni shells, because only when the lattice planes of Au and Ni are parallel or at a very narrow angle can the Moiré Patterns appear in the projection.

By common sense, it is not easy to grow epitaxial Ni layer over an Au surface due to the large difference in lattice spacing. Although, there are a couple of articles in the past reporting the Au@Ni core-shell NPs, the Ni shell is grown by adsorption of Ni nanocrystallites over the Au core and the synthesized NPs are irregular in shape.¹⁷ Nevertheless, the possibility to form Au@Ni NP with Ni grown epitaxially enclosing Au core has been discussed.²⁰ The present work demonstrates that Au@Ni core-shell nanostructures with epitaxial Ni shell are possible.

To explore the growth mechanism of the Au@Ni core-shell nanostructures, the concentration of Ni agent and the time duration of reaction were systematically changed. By reducing the concentration of Ni^{2+} , we found that the initially formed Au NPs are not completely or uniformly covered by Ni layer, as shown in Fig. 5a and b. Alternatively, by collecting the samples at an early stage of reaction, non-uniform Ni shell layer is also observed, as shown in Fig. 5c. At the initial stage of reaction, the Ni layer is grown into island-like areas right on each (111) facet of Au icosahedron. By increasing the concentration of Ni^{2+} or prolonging the reaction time, the Ni islands grow larger and form grain boundaries and defects around adjacent (111) facets. These grain boundaries and defects will prevent further growth of Ni islands and uniform Ni shells will form, as shown in Fig. 5d. This provides further evidence supporting the epitaxial growth of the Ni layers.

Fig. 5e–g are simple diagrams for the phase formation of the Au@Ni icosahedral NPs. The Ni layers first grow epitaxially

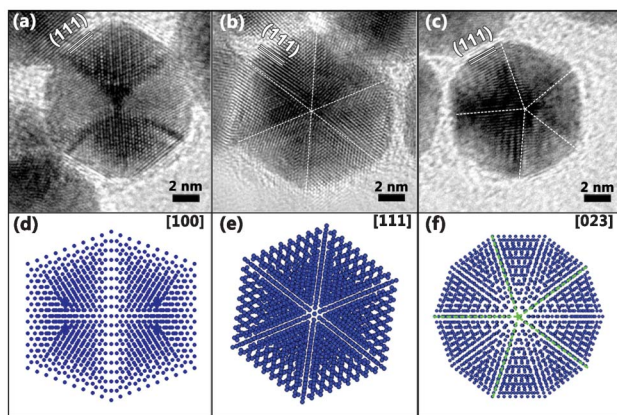


Fig. 3 (a) 2-fold (b) 3-fold and (c) 5-fold symmetry projection of Au icosahedral NP and corresponding atomic simulation images (d), (e) and (f).

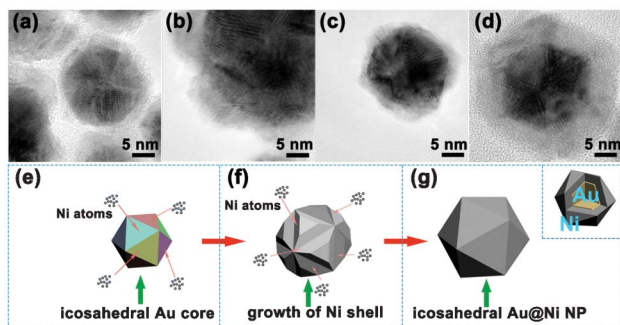


Fig. 5 (a and b) TEM images for the products prepared with 0.012 mmol nickel nitrate; (c and d) TEM images for the intermediates with different reaction duration performed at $T = 185\text{ }^{\circ}\text{C}$ for (c) 10 min and (d) 30 min; HRTEM; (e–g) simulation of the formation process of icosahedral Au@Ni NP.

along the $[111]$ direction on the (111) facets of Au icosahedron after the Au NPs are formed, as revealed by Fig. 5e for the Au NP and Fig. 5f for the early stage of the Ni epitaxial layer grown non-uniformly over the Au (111) facets. As long as the reaction is long enough or the concentration of Ni^{2+} is high enough, the Ni layers grow to form uniform shells. Fig. 5g is a sketch of an Au@Ni icosahedral NP.

Magnetic properties

The magnetization was investigated using a SQUID magnetometer. The temperature dependent magnetization, $M(T)$, curves are shown in Fig. 6a. The FC and ZFC curves would extrapolate to cross each other at a higher temperature, in the range of 350 to 400 K. It implies T_C is smaller than 400 K. Usually, the maximum point in the ZFC curve marks the blocking temperature, T_B . For example, the peak position revealed in the ZFC curve presented in Fig. 2 of ref. 29. With further extension of the ZFC and FC curves in the same figure to higher temperature, the intersection point is a good estimation for the Curie temperature at which the magnetic anisotropy energy approaches zero. This is also the case in Fig. 3 of ref. 30. In some cases, T_B is only slightly lower than T_C as revealed with Mn_3O_4 ,³¹ whereas in the others, T_B is much lower than T_C as is the case for superparamagnetic nanoparticles elaborated in the literature.³² In the present work, the estimated T_C is far less than the bulk Curie temperature of Ni, $\sim 631\text{ K}$. However, by accounting for the finite size effect with the shell thickness of Ni as 5 nm, T_C is estimated to be 339 K

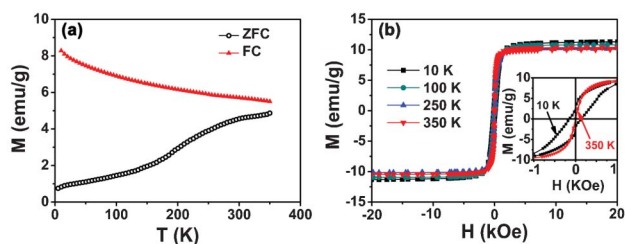


Fig. 6 (a) ZFC-FC curves obtained in measuring and cooling fields of 100 Oe; (b) the hysteresis loops measured at 10 K, 100 K, 250 K and 350 K.

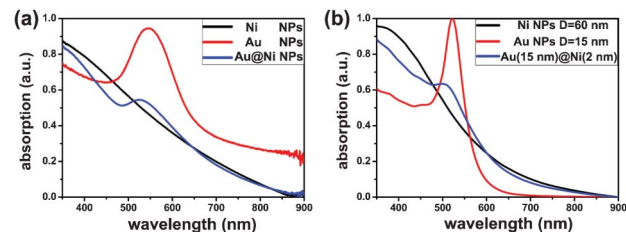


Fig. 7 (a) UV-visible absorption spectra of as-prepared Ni, Au and Au@Ni NPs; (b) calculated UV-visible absorption spectra of Ni ($D = 60\text{ nm}$), Au ($D = 15\text{ nm}$) and Au@Ni (Au core = 15 nm, Ni shell = 2 nm) NPs.

by using the following parameters for Ni, $\zeta_0 \sim 2.2\text{ nm}$ as the correlation length, and $\lambda = 1/\nu = 0.94$ as the shift exponent.^{33,34} The hysteresis loops were measured at 10 K, 100 K, 250 K and 350 K, shown in Fig. 6b. The coercivity is thus determined as 138, 43, 35 and 2 Oe, respectively. It is apparent that the coercivity approaches zero as T reaches the Curie point above 350 K or so. It is worth mentioning that the apparent coercivity thus determined is expected to be reduced owing to the presence of the dipolar interaction effect. Indeed, the hysteresis loops in the inset of Fig. 6b show a sign of distortion with reduced coercivity. This arises from the interparticle dipolar interaction, as explicitly revealed in a previous experiment on the Mn_3O_4 superlattice.³¹

Optical properties

Fig. 7a shows the absorptions of Ni, Au and Au@Ni core-shell NP colloids. The Ni NPs are synthesized by a method similar to our previous experiment³⁵ with the size of $\sim 60\text{ nm}$. In addition, the Au NPs used for the optical measurements are the intermediate as shown in Fig. 1a, while the Au@Ni NPs are the final products as shown in Fig. 1b. The surface plasmon peak of Au appears around 550 nm. The Ni NPs, on the other hand, show a decreased absorption with increasing wavelength, which is consistent to the previous report.³⁶ When the Au is covered by a thin Ni layer, the absorption peak is slightly blue shifted and almost overwhelmed by the optical properties of Ni. This can be understood by the plasmon hybridization theory,³⁷ where the anti-bonding mode from the Au and Ni shell will result in a blue shift depending on the shell thickness.^{38,39} Then, according to particle size measured by the TEM, we perform the calculation based on the generalized Mie theory⁴⁰ as shown in Fig. 7b. Due to the size variation in the experiment, the theoretical absorption predicts a narrow Au peak. However, it is obvious that the spectral blue-shift tendency due to the formation of the core-shell NPs reproduces the experiment very well.

Conclusions

In summary, Au@Ni core-shell nanostructures epitaxial growth of Ni shell layer, 2–5 nm in thickness, enclosing the Au cores of 10–20 nm in diameter, have been synthesized *via* a one-pot chemical method. For the controllable synthesis, sodium citrate played an important role in tailoring the shape

and size of Au cores, while the Ni(OH)₂ precursor concentration determined the thickness and regularity of the Ni shells. The results are of significance to understand the synergistic effect between noble metal and 3d transition magnetic elements.

For the magnetic properties, the Curie point is $T_c \sim 400$ K, much reduced from the bulk value of 631 K. It is attributable to the finite size effect. The absorption peak of the Au@Ni nanostructures is blue shifted compared to the signal of Au cores without Ni shells. It is explained by the calculation based on the plasmon hybridization theory.

Acknowledgements

This work was supported by the National Basic Research Program of China (no. 2009CB939901 and 2010CB934601), the National Natural Science Foundation of China (no. 11174023, 50971011, 10874006 and 11274004), Beijing Natural Science Foundation (no. 1102025), Research Fund for the Doctoral Program of Higher Education of China (no. 20091102110038) and Special Joint Project of Beijing Municipal Education Commission.

References

- 1 D. C. Powers and T. Ritter, *Nat. Chem.*, 2009, **1**, 302–309.
- 2 H. L. Jiang, T. Akita, T. Ishida, M. Haruta and Q. Xu, *J. Am. Chem. Soc.*, 2011, **133**, 1304–1306.
- 3 J. S. Lee, E. V. Shevchenko and D. V. Talapin, *J. Am. Chem. Soc.*, 2008, **130**, 9673–9675.
- 4 Y. Lu, Y. Zhao, L. Yu, L. Dong, C. Shi, M. J. Hu, Y. J. Xu, L. P. Wen and S. H. Yu, *Adv. Mater.*, 2010, **22**, 1407–1411.
- 5 P. K. Jain, I. H. El-Sayed and M. A. El-Sayed, *Nano Today*, 2007, **2**, 18–29.
- 6 Y. Lu, Y. D. Yin, Z. Y. Li and Y. N. Xia, *Nano Lett.*, 2002, **2**, 785–788.
- 7 L. Y. Wang, J. Luo, Q. Fan, M. Suzuki, I. S. Suzuki, M. H. Engelhard, Y. H. Lin, N. Kim, J. Q. Wang and C. J. Zhong, *J. Phys. Chem. B*, 2005, **109**, 21593–21601.
- 8 J. L. Lyon, D. A. Fleming, M. B. Stone, P. Schiffer and M. E. Williams, *Nano Lett.*, 2004, **4**, 719–723.
- 9 D. I. Enache, J. K. Edwards, P. Landon, B. Solsona-Espriu, A. F. Carley, A. A. Herzing, M. Watanabe, C. J. Kiely, D. W. Knight and G. J. Hutchings, *Science*, 2006, **311**, 362–365.
- 10 J. F. Li, Y. F. Huang, Y. Ding, Z. L. Yang, S. B. Li, X. S. Zhou, F. R. Fan, W. Zhang, Z. Y. Zhou, D. Y. Wu, B. Ren, Z. L. Wang and Z. Q. Tian, *Nature*, 2010, **464**, 392–395.
- 11 D. Chen, J. J. Li, C. S. Shi, X. W. Du, N. Q. Zhao, J. Sheng and S. Liu, *Chem. Mater.*, 2007, **19**, 3399–3405.
- 12 Q. Sun, S. G. Wang and R. M. Wang, *J. Phys. Chem. C*, 2012, **116**, 5352–5357.
- 13 Z. H. Ban, Y. A. Barnakov, V. O. Golub and C. J. O'Connor, *J. Mater. Chem.*, 2005, **15**, 4660–4662.
- 14 Y. G. Sun, B. Wiley, Z. Y. Li and Y. N. Xia, *J. Am. Chem. Soc.*, 2004, **126**, 9399–9406.
- 15 G. W. Slawinski and F. P. Zamborini, *Langmuir*, 2007, **23**, 10357–10365.
- 16 Q. Sun, Z. Ren, R. M. Wang, N. Wang and X. Cao, *J. Mater. Chem.*, 2011, **21**, 1925–1930.
- 17 C. J. Serpell, J. Cookson, D. Ozkaya and P. D. Beer, *Nat. Chem.*, 2011, **3**, 478–483.
- 18 H. D. She, Y. Z. Chen, X. Z. Chen, K. Zhang, Z. Y. Wang and D. L. Peng, *J. Mater. Chem.*, 2012, **22**, 2757–2765.
- 19 D. Chen, S. Liu, J. J. Li, N. Q. Zhao, C. S. Shi, X. W. Du and J. Sheng, *J. Alloys Compd.*, 2009, **475**, 494–500.
- 20 D. S. Wang and Y. D. Li, *J. Am. Chem. Soc.*, 2010, **132**, 6280–6281.
- 21 M. Tsuji, D. Yamaguchi, M. Matsunaga and K. Ikeda, *Cryst. Growth Des.*, 2011, **11**, 1995–2005.
- 22 R. M. Wang, O. Dmitrieva, M. Farle, G. Dumpich, H. Q. Ye, H. Poppa, R. Kilaas and C. Kisielowski, *Phys. Rev. Lett.*, 2008, **100**, 017205.
- 23 R. M. Wang, H. Z. Zhang, M. Farle and C. Kisielowski, *Nanoscale*, 2009, **1**, 276–279.
- 24 F. Baletto and R. Ferrando, *Rev. Mod. Phys.*, 2005, **77**, 371–423.
- 25 Y. N. Xia, Y. J. Xiong, B. Lim and S. E. Skrabalak, *Angew. Chem., Int. Ed.*, 2009, **48**, 60–103.
- 26 X. L. Ding, C. X. Kan, B. Mo, S. L. Ke, B. Cong, L. H. Xu and J. J. Zhu, *J. Nanopart. Res.*, 2013, **14**, DOI: 10.1007/s11051-012-1000-8.
- 27 B. Lim, Y. J. Xiong and Y. N. Xia, *Angew. Chem., Int. Ed.*, 2007, **46**, 9279–9282.
- 28 D. Seo, C. I. Yoo, J. C. Park, S. M. Park, S. Ryu and H. Song, *Angew. Chem., Int. Ed.*, 2008, **47**, 763–767.
- 29 L. He, C. P. Chen, F. Liang, N. Wang and L. Guo, *Phys. Rev. B: Condens. Matter Mater. Phys.*, 2007, **75**, 214418.
- 30 C. P. Chen, L. He, L. Lai, H. Zhang, J. Lu, L. Guo and Y. D. Li, *J. Phys.: Condens. Matter*, 2009, **21**, 145601.
- 31 W. M. Chen, C. P. Chen and L. Guo, *J. Appl. Phys.*, 2010, **108**, 043912.
- 32 L. He and C. P. Chen, *Phys. Rev. B: Condens. Matter Mater. Phys.*, 2007, **75**, 184424.
- 33 L. Sun, P. C. Searson and C. L. Chien, *Phys. Rev. B: Condens. Matter*, 2000, **61**, R6463–R6466.
- 34 L. Sun, C. L. Chien and P. C. Searson, *J. Mater. Sci.*, 2000, **35**, 1097–1103.
- 35 P. W. Li, W. M. Chen, W. Liu, Z. A. Li, Y. M. Cui, A. P. Huang, R. M. Wang and C. P. Chen, *J. Phys. Chem. C*, 2010, **114**, 7721–7726.
- 36 J. N. Chen, P. Albella, Z. Pirzadeh, P. Alonso-Gonzalez, F. Huth, S. Bonetti, V. Bonanni, J. Akerman, J. Nogues, P. Vavassori, A. Dmitriev, J. Aizpurua and R. Hillenbrand, *Small*, 2011, **7**, 2341–2347.
- 37 E. Prodan, C. Radloff, N. J. Halas and P. Nordlander, *Science*, 2003, **302**, 419–422.
- 38 H. F. Han, Y. Fang, Z. P. Li and H. X. Xu, *Appl. Phys. Lett.*, 2008, **92**, 023116.
- 39 Y. R. Chen, H. H. Wu, Z. P. Li, P. J. Wang, L. K. Yang and Y. Fang, *Plasmonics*, 2012, **7**, 509–513.
- 40 Z. P. Li and H. X. Xu, *J. Quant. Spectrosc. Radiat. Transfer*, 2007, **103**, 394–401.